Commun. Comput. Phys.
doi: 10.4208/cicp.290711.180711s

Vol. **13**, No. 1, pp. 129-149
January 2013

Effect of the Reaction Field on Molecular Forces and Torques Revealed by an Image-Charge Solvation Model

Wei Song[1], Yuchun Lin[2,3], Andrij Baumketner[2,4], Shaozhong Deng[3], Wei Cai[3] and Donald J. Jacobs[2,*]

[1] *Departments of Bioinformatics and Genomics, University of North Carolina at Charlotte, Charlotte, NC 28262, USA.*
[2] *Departments of Physics and Optical Science, University of North Carolina at Charlotte, Charlotte, NC 28262, USA.*
[3] *Departments of Mathematics and Statistics, University of North Carolina at Charlotte, Charlotte, NC 28262, USA.*
[4] *On leave from Institute for Condensed Matter Physics, 1 Svientsitsky Str., Lviv 79011, Ukraine.*

Received 29 July 2011; Accepted (in revised version) 18 July 2011

Available online 12 June 2012

Abstract. We recently developed the Image-Charge Solvation Model (ICSM), which is an explicit/implicit hybrid model to accurately account for long-range electrostatic forces in molecular dynamics simulations [Lin et al., J. Chem. Phys., 131, 154103, 2009]. The ICSM has a productive spherical volume within the simulation cell for which key physical properties of bulk water are reproduced, such as density, radial distribution function, diffusion constants and dielectric properties. Although the reaction field (RF) is essential, it typically accounts for less than 2% of the total electrostatic force on a water molecule. This observation motivates investigating further the role of the RF within the ICSM. In this report we focus on distributions of forces and torques on water molecules as a function of distance from the origin and make extensive tests over a range of model parameters where Coulomb forces are decomposed into direct interactions from waters modeled explicitly and the RF. Molecular torques due to the RF typically account for 20% of the total torque, revealing why the RF plays an important role in the dielectric properties of simulated water. Moreover, it becomes clear that the buffer layer in the ICSM is essential to mitigate artifacts caused by the discontinuous change in dielectric constants at the explicit/implicit interface.

PACS: 61.20.Gy, 61.20.Ja, 41.20.Cv, 83.10.Rs

Key words: Image charges, reaction field, force distribution, torque distribution, dipole moment.

*Corresponding author. *Email addresses:* wsong4@uncc.edu (W. Song), yuchun.lin@berkeley.edu (Y. Lin), abaumket@uncc.edu (A. Baumketner), shaodeng@uncc.edu (S. Deng), wcai@uncc.edu (W. Cai), djacobs1@uncc.edu (D. J. Jacobs)

1 Introduction

Over the last forty years, better algorithms, faster computers, distributed parallel computing and user-friendly software all contributed [1, 2] to molecular dynamics (MD) becoming an indispensable tool in detailed studies of biopolymers, aimed at gaining insight into mechanisms responsible for biological function [3]. Due to the long-range nature of electrostatic forces, they constitute the key component of MD simulations, affecting the overall speed and accuracy of the method. High accuracy is often needed because electrostatic interactions between molecules are important in biological processes, including signal transmission, ion-transport, molecular recognition, stability and function of biopolymers such as DNA, RNA and proteins. On the other hand, computational cost must be reduced to robustly reach biologically relevant time scales.

The latter consideration motivates the development of implicit solvent models that treat the solute in atomic detail and the solvent as a dielectric continuum to eliminate the molecular degrees of freedom associated with the solvent. A common approach is to solve the linearized Poisson-Boltzmann (LPB) equations to model the effects of the solvent on the solute [4–7]. However, it suffers from two main drawbacks: 1) atomic details of solvent near the surface of solute molecules are neglected where atomic details could be critically important [8], and, 2) the discontinuous change in the dielectric constants at the implicit solvent boundary is a mathematical idealization that leads to artifacts in the electric field within the solute [9]. The alternative approach is the explicit solvent model with full atomic detail for both solute and solvent, which typically employs periodic boundary conditions. A range of explicit solvent methods exist that calculate the electrostatic forces using simple cutoff [10], Ewald summation [11,12], particle-mesh Ewald (PME) [13,14], particle-particle particle-mesh [15,16] and the fast multipole method (FMM) [17–19]. However, for a small simulation box the electrostatic interactions between particles in different periodic image boxes can introduce artifacts [20]. The simple solution to this problem is to increase the box size, but this will incur more computational cost, perhaps to a point of being impractical.

Combining the implicit and explicit approaches, many hybrid models have been [7, 21–23] introduced going back to Kirkwood [24]. However, much care is needed to maintain the homogeneous properties of bulk water while using a hybrid approach because many subtle problems arise due to boundary conditions. We devised the Image-Charge Solvation Model (ICSM) [25] to address these concerns. The ICSM faithfully reproduces the properties of bulk TIP3P waters [26], and solvation free energies, and other key physical properties such as radial distribution functions for the sodium and chlorine ions compared to accurate explicit models [27]. Using more image charges systematically increases the accuracy of the RF within the ICSM. We found that one image charge is sufficient to reproduce bulk water properties at temperatures near 300 K. Interestingly, the relative contribution of the forces from the RF are typically less than 2%. Nevertheless, when the RF is turned off (no image charges used), the dielectric response deviates far from that of bulk water, while structural properties are only marginally affected. These

observations motivated us to investigate the effect of the RF on the forces and torques on water molecules in bulk water, and to further characterize the ICSM. We find that the RF is critical to maintaining the correct molecular torque, explaining the sensitivity on the dielectric response of water.

The remainder of the paper is laid out as follows. In Section 2, we briefly summarize the ICSM, and describe model variations that we further test. In Section 3, we define the methods employed. In Section 4, we present and analyze results for molecular forces and torques on water molecules under a variety of model situations. Finally, we give conclusions in Section 5.

2 Image charge solvation model (ICSM)

Details of the ICSM can be found in previous publications [25, 27]. Here, an overview of the ICSM is given where key features that differ from other hybrid models are highlighted. The ICSM is setup as shown in Fig. 1. The total electrostatic potential $\Phi(r)$ satisfies the LPB equations:

$$\varepsilon_i \nabla^2 \Phi(r) = -\rho_{in}(r), \qquad r \in V_{in}, \tag{2.1a}$$

$$\left[\nabla^2 - \lambda^2\right] \Phi(r) = 0, \qquad r \in V_{out}, \tag{2.1b}$$

where the charge distribution $\rho_{in}(r)$ contains all the explicit charges from solute and solvent molecules, and λ is the inverse Debye-Huckel screening length. For boundary conditions at the spherical surface,

$$\Phi_{in} = \Phi_{out}, \quad \text{and} \quad \varepsilon_i \frac{\partial \Phi_{in}(r)}{\partial n} = \varepsilon_o \frac{\partial \Phi_{out}(r)}{\partial n}, \tag{2.2}$$

where n is the outward normal of the surface. In the work of this paper, we are studying pure water, with $\lambda = 0$.

We apply periodic boundary conditions to short-range forces using a truncated octahedron, which we refer to as a TO-box. A TO-box is generated from a cube of length L by cutting its eight corners at a distance $\sqrt{2}L/4$ from the center. The TO-box has 8 hexagonal and 6 square faces. The distance from the origin to the square face is $L/2$, to the hexagonal face $\sqrt{3}L/4$, and to the corners $R_c = \sqrt{5}L/4$. The short-range forces and local structure of water are modeled well using periodic boundaries because surface effects are minimized. Most other hybrid models use finite boundary [21, 22, 28] conditions, which makes reproducing bulk properties of water near the edge very difficult if not impossible. The ICSM encompasses the TO-box in the spherical cavity, and the TO-box is surrounded by a buffer layer that extends to the spherical cavity wall, where its length is characterized by the radius of the sphere given by $R = R_c + \tau$. The spherical cavity separates two types of dielectric medium where the dielectric constants on the inside, ε_i, and outside, ε_o, of the sphere are respectively set to values for vacuum and bulk solvent, the latter being water in this case.

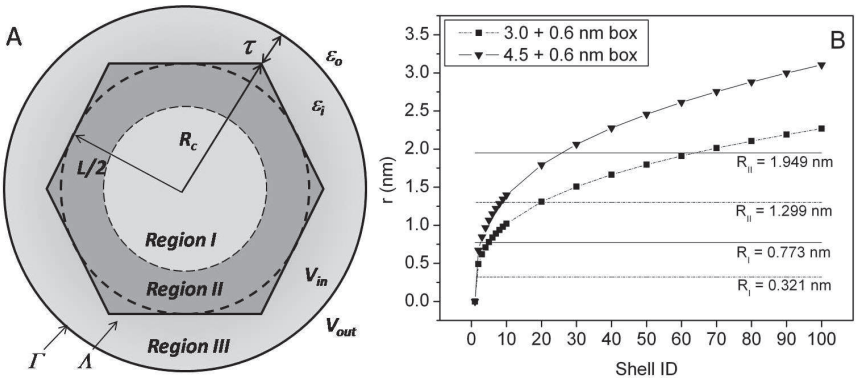

Figure 1: A: Schematic representation showing how the simulation box for the ICSM is divided into three parts inside the spherical cavity of volume, Λ, and surface area, Γ. Regions I and II fill the space within the truncated octahedron box (TO-box) that is placed at the center of the spherical cavity. Region III fills the remaining space as a buffer layer within the spherical cavity and outside the TO-box characterized by length, τ. The water molecules in Region II are imaged into region III using periodic boundary conditions applied to the TO-box. Therefore, water molecules in region III are not associated with dynamic equations of motion. Region I defines the productive volume for simulations, processing translationally invariant properties of bulk water consistent with simulations in large periodic systems. In practice, the majority of region II also represents bulk water well. B: The location of each shell compared with the sizes of regions I and II for different simulation boxes, 30 Å (dash lines) and 45 Å (solid lines).

There are many ways to calculate the RF within hybrid methods. Common methods solve the LPB equation numerically [29], employ approximate theories [21,30], apply an exact series expansion [24,31] for spherical cavities, or use an image charge method [32]. Although the Kirkwood expansion produces arbitrary accuracy of reaction field, it is slow to converge near the boundary [33]. Alternatively, the reaction field can be created by image charges placed outside of the physical domain in the region of the continuum dielectric medium. Friedman [32] gave an approximation for the image charges that can achieve a good accuracy of $O(1/\varepsilon)$ when the dielectric constant is high. Later a more accurate approximation was implemented by Abagyan and Totrov [12] that involved the classical Kelvin image charge for a perfect conductor [34]. However, an exact image charge solution for a dielectric sphere [35–38] expresses the RF potential in terms of a Kelvin image charge plus a radial line image charge extending form Kelvin image charge to infinity. As explained next, this line charge can be represented by a finite number of image charge points. A comparison between these different image charge methods has been reviewed previously [39].

The ICSM is based on a more complete multiple image charge method [39,40]. For each source charge, there is an associated set of image charges placed outside of the sphere along a ray as depicted in Fig. 2 along the radial direction defined by the source point charge. The image charges along this ray give a systematic approximation to the exact image charge solution involving a Kelvin charge (defined for a perfect conductor) plus a continuous line charge that falls off as a power law starting from the Kelvin charge

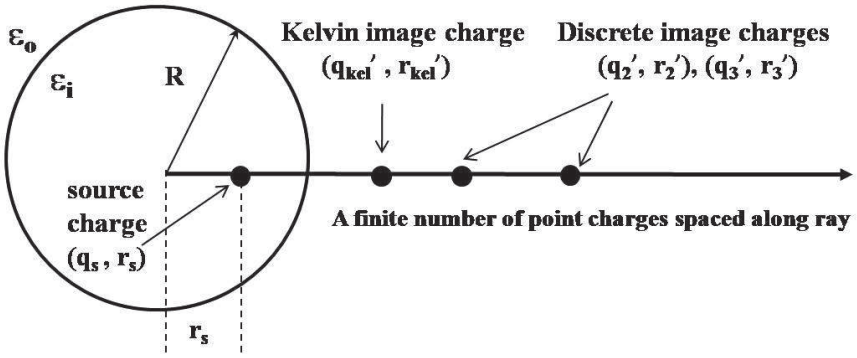

Figure 2: Schematic representation that shows how multiple image charges are placed along a ray on the outside of the spherical cavity to represent the reaction field. Three image charges are used in this case. Note that the location of the Kelvin charge is the same as that for the Kelvin image charge used for a perfect conductor, where the continuous line image charge is zero. Depending on the type of numerical quadrature employed, the value of the charge placed at the Kelvin position will generally be different than the Kelvin charge for a perfect conductor. Nevertheless, the first image charge is still referred to as a modified Kelvin charge.

and extending to infinity [39, 40]. The electric field and electrostatic potential from the line charge is represented using M Gauss-Radau quadrature points, where the first image charge is placed at the location of the classic Kelvin image charge. The numerical approximation for the electrostatic potential of the RF is given in Eq. (2.3). Notice the superposition of M point image charges has a physically intuitive form, where the locations along the ray and corresponding charge for each image are given in Eq. (2.4).

$$\Phi_{RF}(\vec{r}) \approx \frac{q'_K}{4\pi\varepsilon_i|\vec{r}-\vec{r}_K|} + \sum_{m=2}^{M} \frac{q'_m}{4\pi\varepsilon_i|\vec{r}-\vec{r}_m|}, \tag{2.3}$$

$$r_m = r_K\left(\frac{2}{1-s_m}\right)^{1+\frac{\varepsilon_i}{\varepsilon_o}}, \qquad q'_K = \left(1+\frac{\omega_1\varepsilon_i}{2\varepsilon_o}\right)q_K, \qquad q'_m = \frac{\gamma\varepsilon_i}{2\varepsilon_o}\frac{\omega_m r_m}{R}q. \tag{2.4}$$

Here, $r_K = R^2/r_s$ is the distance from the origin to the Kelvin image of charge $q_K = \gamma Rq/r_s$ when the source charge is r_s distance from the origin and has charge q. The discontinuous mismatch in dielectric constants is reflected in the scale factor, $\gamma = (\varepsilon_i - \varepsilon_o)/(\varepsilon_i + \varepsilon_o)$. By employing the Gauss-Radau quadrature, where $\{s_m, \omega_m\}$ for $1 \leqslant m \leqslant M$ are the locations and weights [40] the Kelvin image charge is modified, which is denoted as q'_K. Once the image charges are generated, pairwise forces between all source and all image charges must be summed. The ICSM performs this sum efficiently, scaling as $O(N)$, using recent and very efficient FMM implementations [41–43].

To minimize computational cost, it is desirable to place the cavity boundary that separates the implicit solvent from the simulation space of explicit molecules as close as possible to the TO-box boundary. Because it is common to use the molecular surface of a solute molecule of interest as the boundary between two dielectric media, it is natural to view the space between the TO-box and the boundary of the spherical cavity as wasted.

Leaving this space as vacuum makes the properties of water deviate far from known results. Instead, periodic boundary conditions on the TO-box are used to fill this space with imaged water. Based on previous systematic MD simulations, the optimal range of τ is between 4 to 6 Å, which gives some flexibility on speed/accuracy tradeoff. This range is largely independent of the size of the TO-box. Moreover, the rate at which accuracy is lost below 4 Å is large. Conversely, little gain is seen in accuracy beyond 6 Å. As the buffer layer is increased, additional computational cost is incurred because the atomic charges from the imaged water in the buffer region produce image charges outside the spherical cavity. However, because the water in this buffer region is imaged, it does not require additional equations of motion of its own. The buffer layer characterized by thickness τ allows the diverging values of the RF (near the interface due to the discontinuous dielectric constants) to be ignored entirely. Therefore, the buffer layer is critical to shield the artifacts induced by the explicit/implicit interface.

The boundary condition applied to water molecules at the surface of the spherical cavity may be important, as they may change the nature of the artifacts from the explicit/implicit interface. Three common boundary conditions are considered: Atom-based, group-based and Orientational Disorder Limit (ODL) based rules [44,45], as summarized in Fig. 3. The atom-based rule takes into account Coulomb interactions for atoms within the spherical cavity independent of the location of the other atoms within the same water molecules. The group-based rule considers all charges of the water molecule inside or outside of the spherical cavity based only on if the oxygen atom is inside or outside. This group-based rule was implemented initially in the study of bulk water [25]. The ODL-based rule treats a water molecule as a sphere, and if the entire sphere is inside the spherical cavity, then all atoms within the water molecule are inside the cavity, otherwise outside. In our application to calculating solvation free energy of ions, the ODL-based rules reduced the finite size corrections needed for ion solvation free energy [27]. In other related work, it was found that the group-based rule creates large errors that are not present when atom-based rules are employed [46]. However, this difference becomes apparent when there is net charge on various molecular groups. In the case of water, the differences are not expected to show up. Indeed, within the ICSM for water solvent most quantities are insensitive to the boundary condition used.

3 Methods

Histogram distributions for electrostatic forces and torques on water molecules are constructed based on MD trajectories derived from the simulation of bulk water in thermodynamic equilibrium at room temperature ($T = 300$ K) using ICSM. The Tip3p water model is used [26], in which oxygen atom has a charge of -0.834 and hydrogen 0.417. The length of HO bond is fixed at 0.9572 Å. All details for performing the MD simulations in this work are as published previously [25]. After equilibration, typical MD trajectories are 4 to 6 ns long, and frames were sampled at 0.2 ps apart.

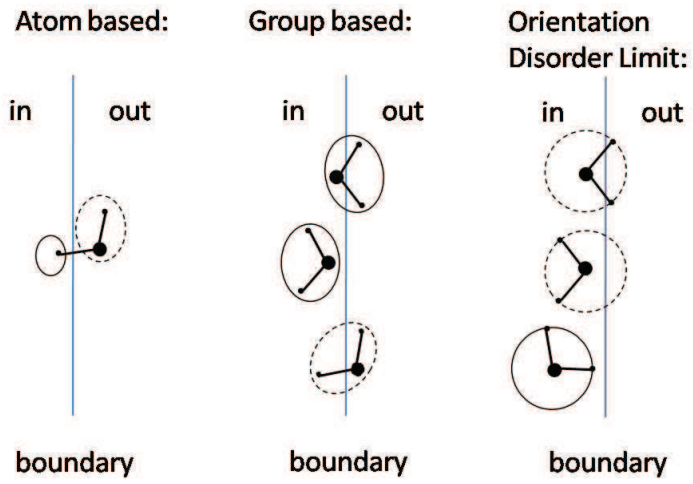

Figure 3: Three different boundary conditions have been applied to water molecules at the surface of the spherical cavity, which is represented as a grey vertical line. Water molecules are drawn as solid circles connected by lines. A (solid, dashed) ellipse or circle indicates which atoms of the water molecule are treated (explicitly inside, implicitly outside) the cavity boundary.

The net force on a water molecule is the sum of pairwise forces on all its atoms. The pairwise force is given by:

$$\vec{F}=\frac{1}{4\pi\varepsilon_i}\left(\frac{Q_1Q_2}{|r|^3}\right)\vec{r}$$

whether it is a direct interaction between atoms, or indirect interaction between atoms and image charges that reside outside of the spherical cavity. The water in the buffer layer is considered as contributing to the direct part of the electrostatic force. The RF derives from a linear superposition of all forces from the image charges that lie outside the spherical cavity. The torque on a water molecule is given as:

$$\overrightarrow{\Gamma}=(\overrightarrow{r_{H_1}}-\overrightarrow{r_{CM}})\times\overrightarrow{F_{H_1}}+(\overrightarrow{r_{H_2}}-\overrightarrow{r_{CM}})\times\overrightarrow{F_{H_2}}+(\overrightarrow{r_O}-\overrightarrow{r_{CM}})\times\overrightarrow{F_O}, \tag{3.1}$$

where $\overrightarrow{r_{CM}}$ is the center of mass of the water molecule, and $\overrightarrow{F_O}$, $\overrightarrow{F_{H_1}}$, $\overrightarrow{F_{H_2}}$ are the electrostatic forces on the oxygen and two hydrogen atoms.

Different types of distributions for forces and torques on water molecules are calculated. The first type of distribution is for the magnitude of the net forces and torques from electrostatic interactions only (no van der Waals forces are included). The second type of distribution is when these forces and torques are broken down into the direct and indirect parts. The third type of distribution is for the radial component of these forces and torques, given by: $F_r=\overrightarrow{F}\cdot\hat{r}$ and $\Gamma_r=\overrightarrow{\Gamma}\cdot\hat{r}$. All three types of distributions are generated for TO-box sizes of $L=30$ Å and $L=45$ Å, atom-based, group-based and ODL-based molecular boundary rules, and for 0, 1, 2 and 3 image charges per source charge.

The distributions are generated for water molecules as a function of distance away from the origin in the form of shells to check how homogeneous the water properties are throughout the TO-box. That is, the spherical cavity is divided into 100 concentric shells of equal volume so that each shell contains approximately the same number of water molecules, typically 13 to 15 for 30 Å box, and 29 to 52 for the 45 Å box. For a particular shell, the electrostatic force and torque values of all water molecules in this shell are calculated and augmented over all the frames from the MD trajectory. The advantage of using shell numbers is that the relative position of a shell in systems of different sizes is the same for the same shell number, which makes comparisons easier. All of the forces or torques per molecule are accumulated and used to construct the histogram distribution for a given shell. The same procedure is applied to all shells. If the oxygen atom is inside a particular shell, then the entire water molecule is treated as if it is in that shell. Thus each water molecule belongs to one and only one shell for a given frame, although it moves between shells over the trajectory. Note that although the histograms are normalized, they do not represent probability density functions because we simply binned the data. Normalization means that summing the probability over all the bins yields unity.

4 Results and discussion

4.1 Force dependence on number of images and system size

As shown in Fig. 4, the statistical distribution of total force on a water molecule for a $L=30$ Å TO-box is largely independent of both shell location and the number of image charges per source charge used to represent the RF. The most obvious outlier is for shell 90, which is close to the spherical cavity wall that also defines the outer boundary of shell 100. The force distribution for shells near the spherical cavity boundary within the buffer layer deviate far from the shells located within region I, as illustrated by the result of shell 90. For the 0 image case, a small deviation starts to appear at shell 70. Note that for the $L=30$ Å TO-box, shell 41 is the smallest shell that contains only imaged water within region III. Consequently, the histograms for the magnitude of the net electrostatic force on a water molecule within any shell that lies fully or partly within the TO-box are essentially the same, independent of the number of image charges used per source charge. This result suggests that the number of image charges per source charge (including 0) is not important. If this is the case, then only the buffer layer is playing a significant role in maintaining proper forces within the TO-box.

Histogram distributions are shown in Fig. 5 for the net force on a water molecule that is separated into direct and indirect parts. It is seen that there is strong shell dependence for the RF part, but only a weak dependence on shell position for the direct part, which is associated with all explicit water molecules within the spherical cavity. Simultaneous strong shell dependence on the RF and weak shell dependence on the total force is possible because of separation of scales. The RF forces in comparison to direct forces typically provide less than a 2% effect, which is shell dependent. Within the productive region, the

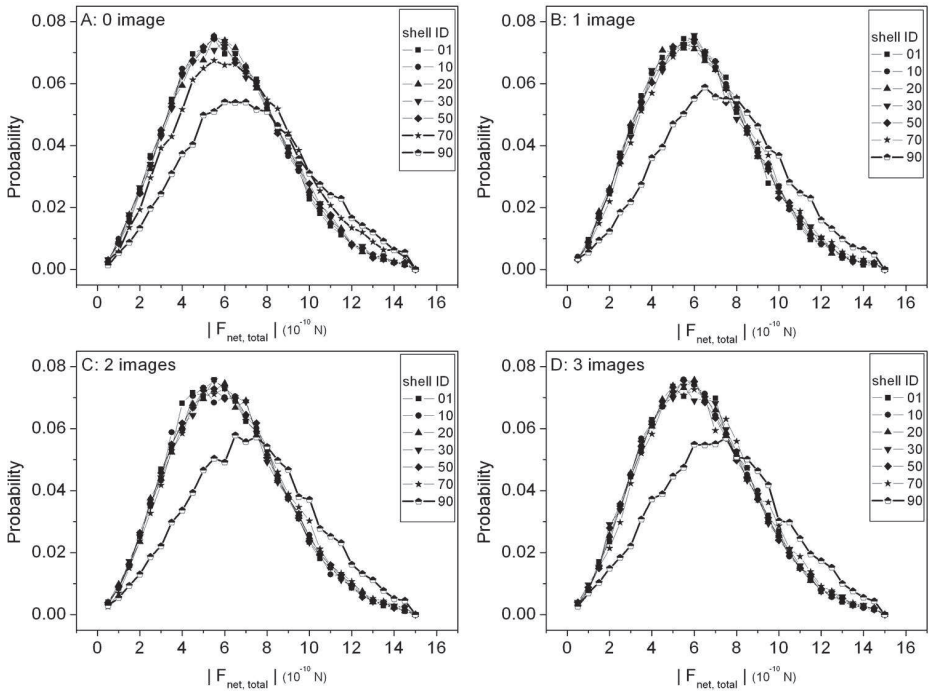

Figure 4: Selected distributions within various shells for the magnitude of the net electrostatic force on a water molecule. The total force consists of direct water interactions and the RF component. A box size of $L=30$ Å and 6 Å buffer layer is used, and the results are shown for different number of images. Note that the distributions are normalized histograms generated using 30 bins of equal size over the range of 0 to 1.5×10^{-10} N.

relative importance is about 1% while at the end of region II the percentage goes as high as 2%. The initial objective for the ICSM was to reproduce correct physical properties of water in the productive region (region I as defined in Fig. 1). Pleasingly, the simulations for bulk water properties [25] and for calculating the ion solvation free energy [27] produced results that preserved homogenous characteristics of the system under study markedly well within the TO-box, which includes region II. Because the relative strength of the direct to indirect RF forces is typically greater than 50, it appears that the main reason why the ICSM does well is because of the buffer layer. This result suggests that the buffer layer should be employed, and perhaps the image charges that control the RF forces are not necessary!

As the shells move further out into the buffer range, the relative contribution is increasing. As shown in Table 1, for shell 70, the contributions of reaction field are 35.6% for 30 Å and 16.4% for 45 Å boxes, while for the first shell they are only 1.0% and 0.6%, respectively. The useful shells in regions I and II are extended outwards using a larger TO-box and the outliers again only occur well within the buffer region. This result shows that the buffer layer made up of imaged water of the TO-box is absorbing large RF forces, but dynamics is not affected by these forces. We tested to see if the buffer layer by itself

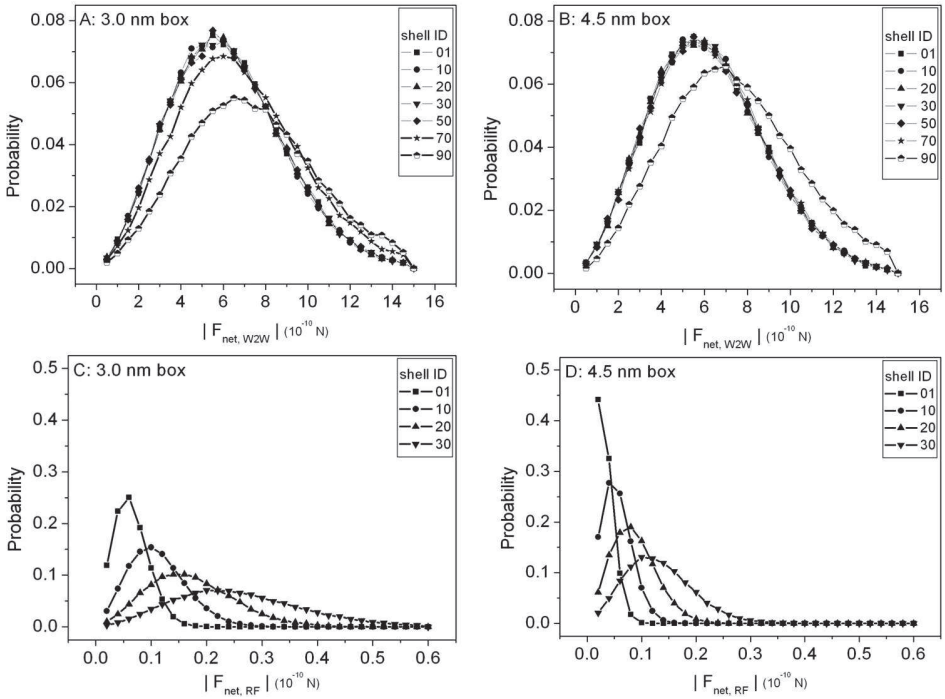

Figure 5: The net electrostatic force is split into two parts originating from direct interactions and from the RF. The bin size for the direct component is the same as used in Fig. 4, and 30 bins of equal size over the range of 0 to 0.6×10^{-10} N was used for the RF component. The top two panels show the direct interactions, while the bottom panels show the RF component of the net force. The left column shows results for the $L=30$ Å TO-box, and the right column shows results for the $L=45$ Å TO-box. Both box sizes use a 6 Å buffer layer.

is sufficient to generate an accurate RF, meaning all image charges in the domain outside of the spherical cavity are simply dropped. After dropping image charges outside the cavity, the buffer layer alone yields very large erroneous results in the dielectric response [25], while other structural properties of water did not deviate much. Moreover, we find that to insure high accuracy in the RF throughout the TO-box, the imaged water in the buffer region must also generate image charges in the domain outside of the cavity (data not shown).

The role of the buffer layer is therefore essential to preserve local structure of water consistent with homogeneous bulk water properties, which includes the long-range electrostatic force that is in part induced by the waters in the buffer layer. This leads to the question, why is the RF essential (using at least one image charge) despite having a relative force contribution that is typically less than 2%? Since the dielectric response is related to the polarization of water, a natural quantity to characterize is the torques on water molecules, which governs the orientation of the permanent electric dipoles. Another question is whether it is possible that the forces and/or torques generated by the RF are sensitive to the particular molecular boundary condition?

Table 1: For different shells, the ratio of the RF part to the total electrostatic forces (RF part + direct part) per water molecule. The unit of force is 10^{-10} N.

Shell ID	30+6 Å Total force	30+6 Å RF force	Ratio RF/Total	45+6 Å Total force	45+6 Å RF force	Ratio Rf/Total
01	7.6640	0.0787	0.010	6.5267	0.0400	0.006
10	7.4940	0.1195	0.016	6.4476	0.0649	0.010
20	7.1199	0.1808	0.025	6.4917	0.0967	0.015
30	6.7418	0.2692	0.040	6.4319	0.1435	0.022
50	6.3996	0.6353	0.100	3.4946	0.3351	0.052
70	6.6274	2.3622	0.356	6.5268	1.0676	0.164

4.2 Force and torque dependence on molecular boundary conditions

No systematic shell dependence on the distributions for forces and torques of any type (i.e. total, direct or RF) were found when different molecular boundary conditions were employed. The two extreme cases are the atom-based and ODL-based rules defined in Fig. 3. In Fig. 6, we show two representative examples of distributions for the radial components of the forces and torques using atom-based and ODL-based rules. Some differences are found in the shells within the buffer layer close to the spherical cavity walls as illustrated by shell 70. However, even qualitative features remain the same (comparing panels C and D for example). Therefore, as far as force and torque distributions are concerned, the molecular boundary rule that is applied along the spherical cavity wall is not important provided the buffer layer is large enough, which was previously determined to be 4 to 6 Å [25]. Within the buffer layer, the differences in forces and torques on the imaged water molecules that depend on the choice of molecular boundaries are not reflected in the dynamics of the molecules. Although data is not shown for group-based boundary rules (the original implementation [25]), in summary, no discernable difference between any of these three boundary conditions is found in the histogram distributions of forces and torques for bulk water.

4.3 Torque dependence on number of images and system size

In Fig. 7, it is shown that for 1 image charge, the histogram distributions for the magnitude of torques that originate from only direct water-to-water interactions carry slight shell dependence. This result is independent of system size. The shell dependence is dramatically increased once the shells enter the buffer region, as expected. Similar histogram distributions are shown for the magnitude of net torques that originate from only the RF. In this case, the shell dependence is very strong throughout the entire spherical cavity, both inside and outside the TO-box — similar to what was found for forces. However, the relative scales are much closer. Whereas the forces from the RF compared to direct interactions is typically a 1% contribution within region I, the torques due to the RF compared to the direct interactions is about a 20% contribution. In Table 2, both to-

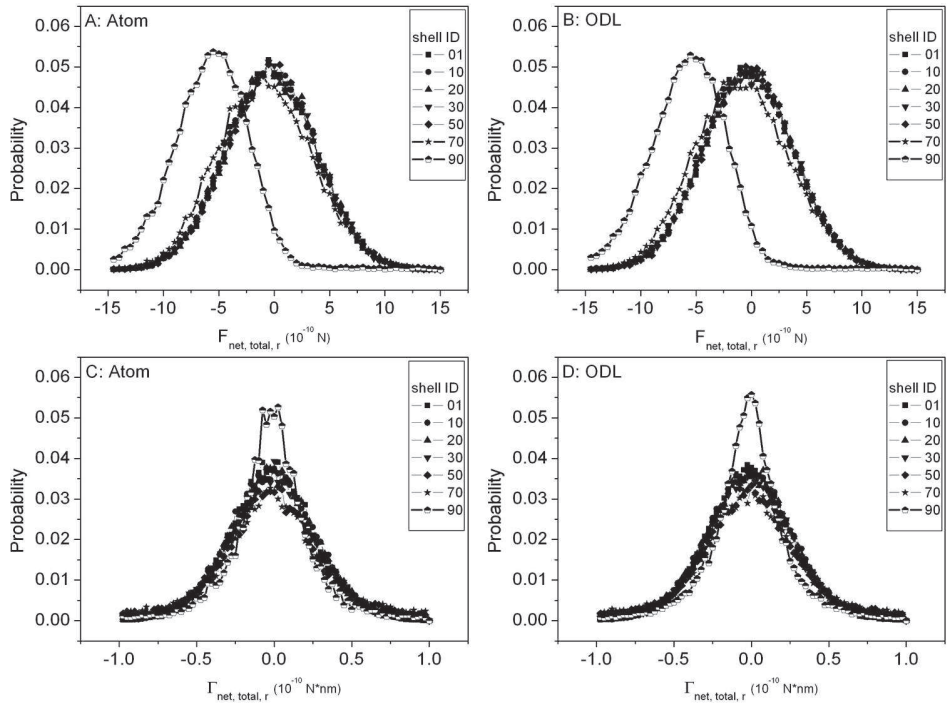

Figure 6: Comparing distributions for the radial component of the total force (shown in top row) and the radial component for the total torque (shown in bottom row) using the $L=30$ Å TO-box and one image charge. The (left, right) columns show the histograms for (atom-, ODL-) based rules.

tal electrostatic torque and torque from reaction field are growing when the size of shell increases. In shell 1, the ratio is 20.8% and 15.1% for 30 Å and 45 Å boxes, respectively. These ratios are much larger than those of electrostatic force shown in Table 1, which are no larger than 2.0% before shell 10. The comparison between Tables 1 and 2 elucidates that, in region I, electrostatic torques from the reaction field play a more important role than electrostatic force to maintain the correct dielectric properties. Therefore, the

Table 2: For different shells, the ratio of the RF part to the total electrostatic torques (RF part + direct part) per water molecule. The unit of torque is 10^{-10} N nm.

Shell ID	30+6 Å Total torque	30+6 Å RF torque	Ratio RF/Total	45+6 Å Total torque	45+6 Å RF torque	Ratio Rf/Total
01	0.4373	0.0910	0.208	0.4479	0.0677	0.151
10	0.4552	0.1127	0.248	0.4368	0.0823	0.188
20	0.4737	0.1346	0.284	0.4374	0.0986	0.225
30	0.5533	0.1610	0.291	0.5140	0.1227	0.239
50	0.7224	0.2773	0.384	0.8412	0.2230	0.265
70	0.7267	0.5059	0.696	0.8469	0.4017	0.474

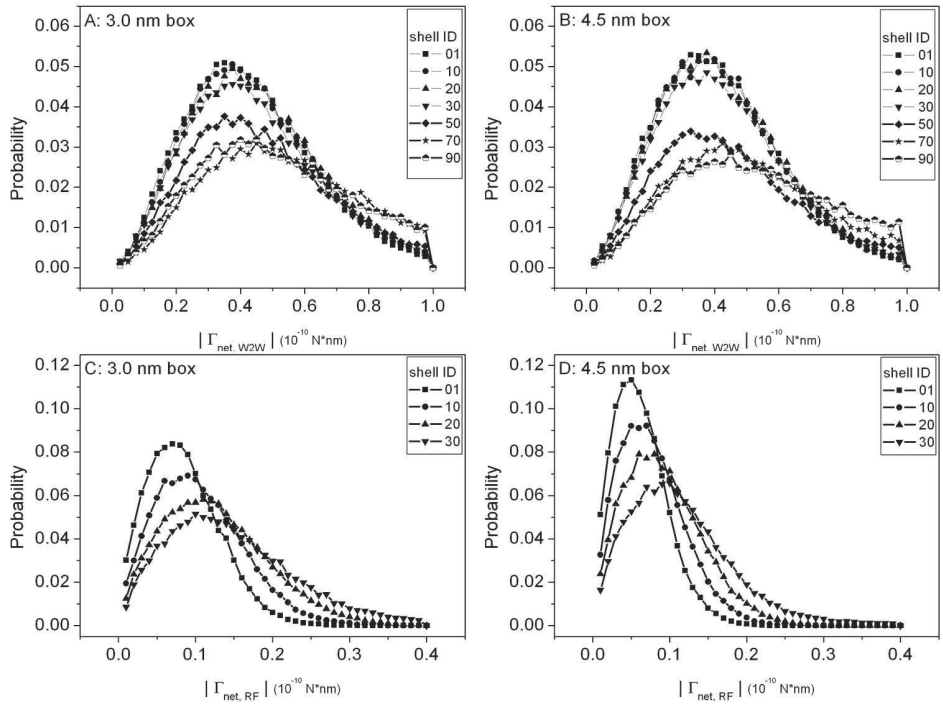

Figure 7: The net torque on water molecules due to electrostatic forces is split into two parts that originate from direct interactions and the RF. To produce the histograms, 40 bins are used over the range 0 to 1×10^{-10} N nm for the direct component, and over the range 0 to 0.4×10^{-10} N nm for the RF component. The top two panels show the results for the direct interactions, while the bottom panels show the results for the RF component of the net torque. The left column shows results for the $L=30$ Å TO-box, and the right column shows results for the $L=45$ Å TO-box. Both box sizes use a 6 Å buffer layer.

importance of the image charges is not related directly to forces, but more specifically to torques, which is responsible for the orientation of the water molecules, and thus the local polarization properties. This result is physically intuitive, and it motivated a further check on the significance of the number of image charges on affecting the torque distributions (recalling forces were not sensitive at all).

In Fig. 8, the effect of using a different number of image charges per source point (0 to 3) on the histogram distributions for net torque that include both direct and RF components are compared for the ODL-based molecular boundary case. It is somewhat surprising to see that the affect of the RF is hardly visible. Using 1 to 3 image charges per source point show virtually no differences within statistical noise. When using no images, a more noticeable change does occur for the outer shells, but no deviation is discernable for any shell up to shell 20, which ends region II. This result again suggests that the buffer layer of imaged water is sufficient to model bulk water, dropping the image charges altogether. As mentioned above, this experiment was indeed performed in earlier work [25]. Most of the physical quantities that was checked did not depend strongly on whether the

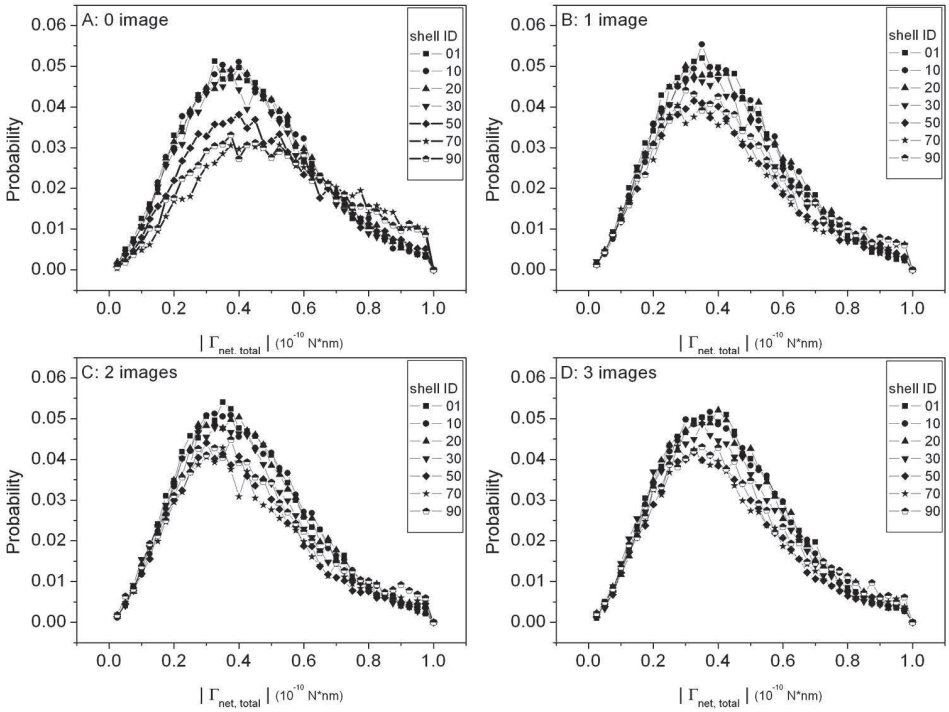

Figure 8: Histogram distributions for the magnitude of the net torque due to the electrostatic forces originating from both the direct and RF parts is shown for four cases invoking 0 to 3 images in the MD simulation using the $L=30$ Å TO-box with a 6 Å buffer layer. To produce the histograms, 40 bins are used over the range 0 to 1×10^{-10} N nm.

image charge was present or not, except for the dielectric constant, which dramatically changed between the 0 and 1 image case. In Fig. 9, similar results are shown only for the radial part of the net torques. It was our expectation that a difference in torque distributions would be detected when comparing the 0 and 1 image charge case. In our previous studies, group-based molecular boundary rules were employed [25], while the results shown here are for ODL-based rules that were incorporated in the ICSM in subsequent work [27]. As we show below, the molecular boundary condition is not the reason for not seeing a difference between the 0 and 1 image charge case.

A possible reason why the torque distributions do not reflect the differences we found earlier between the 0 and 1 image charge cases is because the differences that are present are spatially averaged out by using concentric shells. Even the radial component of the torque distribution is subject to this possibility. However, because the radial pair distribution function (between oxygen atoms) is not very sensitive to using the 0- and 1-image charge cases (data not shown), this implies that during the MD simulation the collective behavior of the water molecules restore the net total forces and torques to statistically support the same histogram distribution. However, this still leaves a perplexing

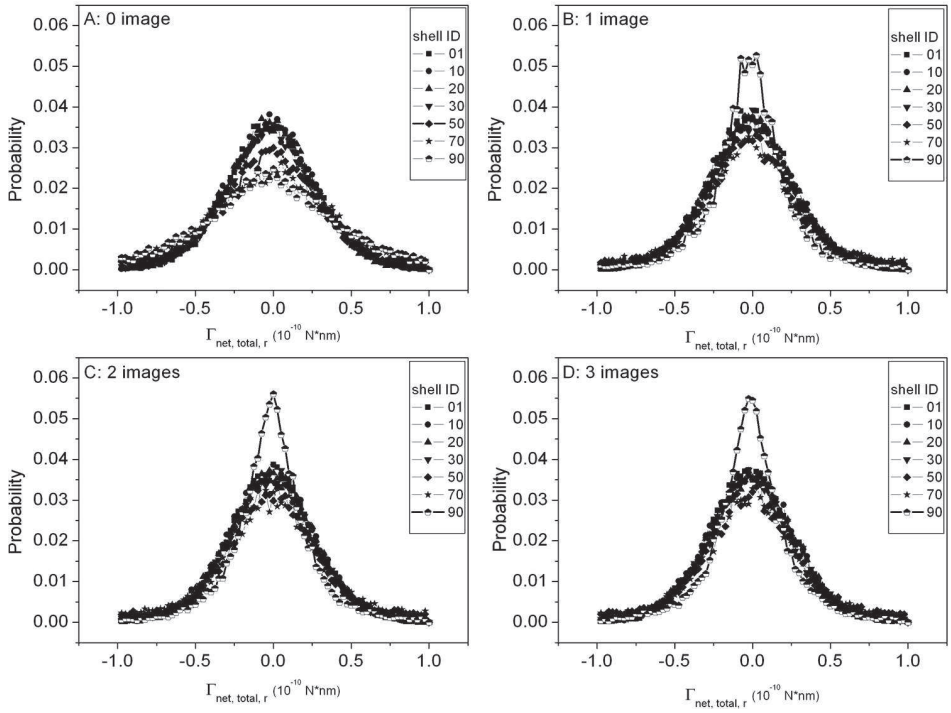

Figure 9: Histogram distributions for the radial component of the net torque due to the electrostatic forces originating from both the direct and RF parts is shown for four cases invoking 0 to 3 images in the MD simulation using the $L=30$ Å TO-box with a 6 Å buffer layer. To produce the histograms, 40 bins are used over the range 0 to 1×10^{-10} N nm.

dilemma, because at least 1 image charge is necessary to maintain the correct dielectric constant. These results suggest that our analysis is missing correlations in orientations between pairs of water molecules.

To demonstrate that there is indeed an important difference between using 0 and 1 image charge per source charge, the net dipole moment for a spherical ball centered at the origin as a function of radius is shown in Fig. 10 for both the atom-based and ODL-based rules applied at the spherical cavity walls. Error bars are calculated to show that $N_i>0$ cases are all equivalent to one another within statistical errors, but these results are very different from the no image charge case ($N_i=0$). The formula for the total dipole moment as a function of radius r with respect to the origin of the TO-box and spherical cavity is given in Eq. (4.1), where a spherical ball contains all water molecules in frame, j, that have its oxygen atom within the radius, r, considered.

$$\left\langle P^2\right\rangle_{total}=\sum_{j=1}^{J}\left\langle \vec{P}_j\cdot\vec{P}_j\right\rangle,\quad \text{where}\quad \vec{P}_j=\sum_{k=1}^{K}\left(q_{O,k}\vec{r}_{O,k,j}+q_{H_1,k}\vec{r}_{H_1,k,j}+q_{H_2,k}\vec{r}_{H_2,k,j}\right). \tag{4.1}$$

The dipole moment is averaged over all J-frames from the MD trajectory, where the atom

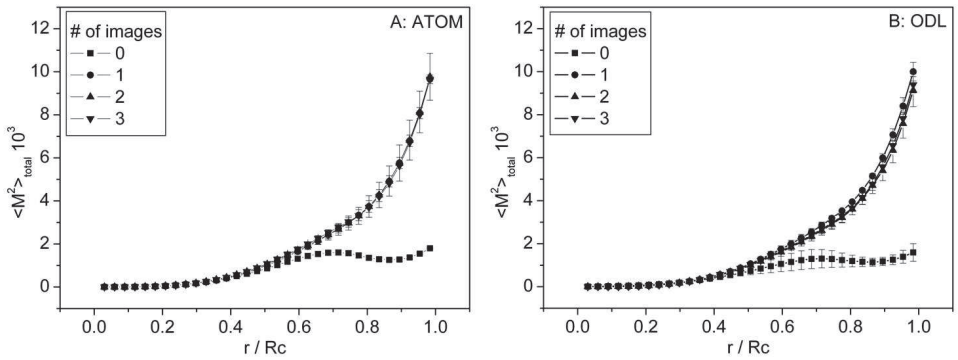

Figure 10: The total dipole moment for spherical balls of radius r is plotted for four cases invoking 0 to 3 images in the MD simulation using the $L=30$ Å TO-box with a 6 Å buffer layer. R_C is defined in Fig. 1A. The overlapping error bars show that $N_i=1$, 2, 3 cases are producing the same results, based on the 6.0 ns trajectory for atom-based and 4.8 ns for ODL-based cases. The error bars on the 0 image curve in the atom-based case are smaller than the size of the symbols. A: Atom-based and B: ODL-based boundary rules are used.

position vectors for the k-th molecule in the j-th frame weight the oxygen and hydrogen atoms. Because the first non-zero multipole is the dipole moment, the result is independent of choice of origin. Thus, the expression given in Eq. (4.1) is equivalent to defining the origin to be at the center of mass or at the oxygen atom for each water molecule.

The total dipole moment is needed to calculate the dielectric constant, and it represents a quantity that reflects fluctuations in the orientations of water molecules that captures correlations that are presumably missed in the torque distributions shown above. This dipole moment calculation was done for both the atom-based and ODL-based boundary rules. These results confirm the previous study using group-based boundary rules. Therefore, any of the three common molecular boundary conditions considered here have little to no influence on the molecular force and torque distributions regarding properties of bulk water. This is not to say that there are not advantages to employ one boundary condition over the other for certain physical quantities or deficiencies may exist in certain cases as pointed out previously [25,46].

The interesting feature identified is that within region I, there is essentially no difference between using 0 or 1 image charge per source charge. The buffer layer on its own already makes region I resemble bulk properties of water. However, region II retains the properties of bulk water as well. As Fig. 10 shows, a non-negligible deviation starts to occur just at the end of region II (a radius of 12.9 Å ends region II for a $L=30$ Å TO-box.). For bulk water simulations [25] and for ion solvation [27], we previously reported that in practice region II also maintained the properties of bulk water well when 1 image charge per source charge is used in the ICSM. For practical purposes, dropping the single image will surely increase unwanted finite size effects because physical correlations involving water orientations will be lost, and therefore is not recommended. Moreover, 1 image charge per source charge appears to be sufficient for high accuracy.

4.4 Importance of the reaction field and the buffer region

Building on prior works [25,27], combined with the above detailed analysis of force and torque distributions, we have shown that the importance of the reaction field manifests directly through the net torques on the water molecules. The RF component represents a long-range effect that works in a subtle way to create correlations in the orientation of water molecules, and thus affects the polarizability of the solvent. The observation that torque plays a central role in describing proper bulk properties of water has been exploited in the local molecular field (LMF) [47] theory approach. In general, boundary conditions that arise at the interfaces between different types of medium are difficult to deal with due to the long-range nature of the electrostatic force. As such, simple cut-off procedures create large errors. These errors have been addressed within the LMF approach [47] by accounting for the net long-range electrostatic forces in terms of reorienting torques on water molecules, which is consistent with our calculations. As such, this suggests that the success of the LMF approach is precisely because the dominant effect has been accounted for.

The results presented above also suggest that if 1 image charge per source charge is kept the buffer layer can be reduced, since all shells maintained the same force and torque distributions within region I and most (if not all) of region II. Although the distributions were not shown, it was already clearly demonstrated [25] that the buffer layer thickness is critical to maintaining accurate structural and dynamic properties of bulk water. As soon as the buffer layer is reduced (say to 4 Å) some properties of water deviate from the desired target properties of bulk water. This prior observation is understandable because the relative importance of both torques and forces from the RF compared to direct interactions increases when a water molecule comes closer to the spherical cavity wall. From a practical point of view, a buffer layer of 4 Å may introduce errors that are tolerable for many applications, but 6 Å will ensure high accuracy whenever needed. This finding leads us to point out a serious concern involving artifacts found in any explicit/implicit model.

The method of images [40] is a rigorous way of solving the Poisson equation for a system with spherical geometry that we have employed in the ICSM. It is worth noting that this method can be extended to accurately solve the linearized Poisson-Boltzmann equation with arbitrary ionic strength [48]. In the case of bulk water, we show here that the Poisson equation can be solved more accurately using multiple images (2 or 3 per source point for example) than is required because the physical quantities that can be calculated do not gain in any detectable accuracy. This is because the discontinuous model for the dielectric to change from within the cavity to the continuous dielectric medium outside of the spherical cavity walls is a mathematical idealization. As such, the forces and torques near this boundary are unphysical. To counter this problem, the buffer layer is introduced to absorb idealized-model induced errors. The buffer layer is therefore an essential part of the ICSM.

It is necessary to use multiple image charges (more than one) for accurate calculation

of the electrostatic forces for charges in the simulation box near the spherical dielectric interface where the Kirkwood expansion converges extremely slowly. However, this region is where the buffer layer is located. The ICSM uses imaged water molecules in the buffer layer, which do not have associated dynamical equations of motions. Although increasing the number of image charges will increase the accuracy of the water molecules within the buffer layer, our results show that the accuracy is already sufficient for the water molecules outside of the buffer layer. In other words, improving accuracy for the forces and torques on water molecules within the buffer layer is not relevant. For fixed buffer layer thickness, as the spherical shell radius increases should lead to a situation that multiple image charges will be needed for very large box sizes. However, even up to an 80 Å box with $\varepsilon_o = 80$, one image charged was found to be sufficient in accuracy [25]. Also, we explored whether more than one image charge is needed for bulk water simulations using different ε_o values that go as low as $\varepsilon_o = 10$. In all cases checked for bulk water, we find one image charge is good enough to recover accurate properties of bulk water. However, also note that this single image charge is slightly modified from the classical Kelvin charge, and partly accounts for the imaged line charge in addition to the classical Kelvin charge.

The significance of a minimum thickness buffer layer to ensure accurate calculations of electrostatic interactions is more far-reaching than a simulation protocol for modeling bulk water. Rather, the analysis presented here demonstrates that any model that employs a discontinuous change in the dielectric constant within the physical domain of interest will create large spurious forces and torques on explicitly modeled atoms. Therefore, when developing a hybrid model that interfaces continuum electrostatics with explicit atomic systems, a buffer layer should be included to better model structural details at the interface [49], and to allow a way for artifacts caused by the unphysical boundary conditions to die out far enough away from the parts of the system that are under study.

5 Conclusion

Molecular forces due to the reaction field are typically less than 2% of the total force, while in comparison, molecular torques due to the reaction field are typically 20% of the total torque. Since molecular torques affect water orientation, and thus polarization, the role of the reaction field is essential in describing the correct molecular response to electrostatic forces. In particular, the reaction field is responsible for generating correlations in the orientations of water molecules, which affects the local dipole moment. In addition, it is shown that using a discontinuous dielectric model produces large artifacts at the interface, which can be essentially removed by applying a buffer layer. The role of the buffer layer used in the ICSM is critical to maintaining high accuracy because the spurious forces and torques that are generated near the interface walls do not affect the dynamics of the molecules near the walls because they are imaged. More generally, the analysis shows that it is important to create a buffer layer in multi-scale hybrid models,

and/or to completely avoid discontinuous change in the dielectric within the physical domain of interest.

Acknowledgments

This work is supported by the National Institutes of Health grants R01 GM083600 and S10 SRR026514.

References

[1] P. Larsson, B. Hess, and E. Lindahl, Algorithm improvements for molecular dynamics simulations, WIREs. Comput. Mol. Sci., 1, 93-108, 2011.
[2] J. Klepeis, K. Lindorff-Larsen, R. Dror, and D. Shaw, Long-timescale molecular dynamics simulations of protein structure and function, Curr. Opin. Struct. Biol., 19, 120-127, 2009.
[3] W. Gunsteren, D. Bakowies, R. Baron, I. Chandrasekhar, M. Christen, X. Daura, P. Gee, D. P. Geerke, A. Glattli, P. H. Hunenberger, M. A. Kastenholz, C. Oostenbrink, M. Schenk, D. Trzesniak, N. Vegt, and H. B. Yu, Biomolecular modeling: Goals, problems, perspectives, Angew. Chem. Int. Ed., 45, 4064-4092, 2006.
[4] J. Wang, C. Tan, Y. Tan, Q. Lu, and R. Luo, Poisson-Boltzmann solvents in molecular dynamics simulations, Commun. Comput. Phys., 3, 1010-1031, 2008.
[5] B. Roux, Implicit solvent models, in Computational Biochemistry and Biophysics, O. M. Dekker, A. D. MacKerell, Jr., B. Roux, M. Watanabe, Ed., New York, 133-150, 2001.
[6] B. Honig and A. Nicholls, Classical electrostatics in biology and chemistry, Science, 268, 1144-1149, 1995.
[7] N. A. Baker, Improving implicit solvent simulations: A Poisson-centric view, Curr. Opin. Struct. Biol., 15, 137-143, 2005.
[8] Z. Yu, M. P. Jacobson, J. Josovitz et al., First-shell solvation of ion pairs: Correction of systematic errors in implicit solvent models, J. Phys. Chem. B, 108, 6643-6654, 2004.
[9] A. Rubinstein and S. Sherman, Influence of the solvent structure on the electrostatic interactions in proteins, Biophys. J., 87, 1544-1557, 2004.
[10] M. P. Allen and D. J. Tildesley, Computer Simulation of Liquids, Oxford University Press, Oxford, 1987.
[11] P. P. Ewald, Die Berechnung optischer und elektrostatischer Gitterpotentiale, Ann. Phys, 369, 253-287, 1921.
[12] R. Abagyan and M. Totrov, Biased probability Monte Carlo conformational searches and electrostatic calculations for peptides and proteins, J. Mol. Biol., 235, 983-1002, 1994.
[13] U. Essmann, L. Perera, M. Berkowitz, T. Darden, H. Lee, and L. Pedersen, A smooth particle mesh Ewald method, J. Chem. Phys., 103, 8577-8593, 1995.
[14] T. A. Darden, D. M. York, and L. G. Pedersen, Particle mesh Ewald: An Nlog(N) method for Ewald sums in large systems, J. Chem. Phys., 98, 10089-10092, 1993.
[15] J. Shimada, H. Kaneko, and T. Takada, Efficient calculations of coulombic interactions in biomolecular simulations with periodic boundary conditions, J. Comput. Chem., 14, 867-878, 1993.
[16] B. Luty, M. Davis, I. Tironi, and W. Gunsteren, A comparison of particle-particle, particle-mesh and Ewald methods for calculating electrostatic interactions in periodic molecular systems, Mol. Simul., 14, 11-20, 1994.

[17] L. Greengard and V. Rokhlin, A fast algorithm for particle simulations, J. Comput. Phys., 73, 325-348, 1987.
[18] L. Greengard, The Rapid Evaluation of Potential Fields in Particle Systems, MIT Press, Cambridge, 1988.
[19] L. Greengard and V. Rokhlin, A new version of the Fast Multipole Method for the Laplace equation in three dimensions, Acta Numerica, 6, 229-269, 1997.
[20] R. Gargallo, P. H. Hunenberger, F. X. Aviles, and B. Oliva, Molecular dynamics simulation of highly charged proteins: Comparison of the particle-particle particle-mesh and reaction field methods for the calculation of electrostatic interactions, Protein Sci., 12, 2161-2172, 2003.
[21] M. Lee, F. Salsbury, and M. Olson, An efficient hybrid explicit/implicit solvent method for biomolecular simulations, J. Comput. Chem., 25, 1967-1978, 2004.
[22] A. Okur and C. Simmerling, Hybrid explicit/implicit solvation methods, Ann. Rep. Comp. Chem., 2, 97-109, 2006.
[23] M. S. Lee and M. A. Olson, Evaluation of Poisson solvation models using a hybrid explicit/implicit solvent method, J. Phys. Chem. B, 109, 5223-5236, 2005.
[24] J. G. Kirkwood, Theory of solutions of molecules containing widely separated charges with special application to Zwitterions, J. Chem. Phys., 2, 351-361, 1934.
[25] Y. Lin, A. Baumketner, S. Deng, Z. Xu, D. J. Jacobs, and W. Cai, An image-based reaction field method for electrostatic interactions in molecular dynamics simulations of aqueous solutions, J. Chem. Phys., 131, 154103, 2009.
[26] W. L. Jorgensen, J. Chandrasekhar, J. D. Madura, R. W. Impey, and M. L. Klein, Comparison of simple potential functions for simulating liquid water, J. Chem. Phys., 79, 926-935, 1983.
[27] Y. Lin, A. Baumketner, W. Song, S. Deng, D. Jacobs, and W. Cai, Ionic solvation studied by image-charge reaction field method, J. Chem. Phys., 134, 3530094, 2011.
[28] D. Beglov and B. Roux, Finite representation of an infinite bulk system: Solvent boundary potential for computer simulations, J. Chem. Phys.,100, 9050, 1994.
[29] W. Im, S. Berneche, and B. Roux, Generalized solvent boundary potential for computer simulations, J. Chem. Phys., 114, 2924, 2001.
[30] D. Bashford and D. Case, Generalized Born models of macromolecular solvation effects, Ann. Rev. Phys. Chem., 51, 129-152, 2000.
[31] J. Kirkwood, Statistical mechanics of liquid solutions, Chem. Rev., 19, 275-307, 1936.
[32] H. Friedman, Image approximation to the reaction field, Mol. Phys., 29, 1533-1543, 1975.
[33] I. G. Tironi, R. Sperb, and P. E. Smith, Generalized reaction field method for molecular dynamics simulations, J. Chem. Phys., 102, 5451-5459, 1995.
[34] P. M. Morse and H. Feshbach, Methods of Theoretical Physics, McGraw-Hill, New York,, 1953.
[35] C. Neumann, Hydrodynamische untersuchen nebst einem anhang uber die probleme der elektrostatik und der magnetischen induktion, Teubner, Leipzig, 279, 1883.
[36] A. V. Finkelstein, Electrostatic interactions of charged groups in an aqueous medium and their effect on the formation of polypeptide chain secondary structure, Mol. Biol., 11, 811, 1977.
[37] I. V. Lindell, Electrostatic image theory for the dielectric sphere, Radio Sci., 27, 1-8, 1992.
[38] W. T. Norris, Charge images in a dielectric sphere, IEE Proc.: Sci., Meas. Technol., 142, 142-150, 1995.
[39] S. Deng, W. Cai, and D. J. Jacobs, A comparable study of image approximations to the reaction field, Comput. Phys. Commun., 177, 689-699, 2007.
[40] W. Cai, S. Deng, and D. J. Jacobs, Extending the fast multipole method to charges inside or

outside a dielectric sphere, J. Comput. Phys., 223, 846, 2007.
[41] B. Zhang, J. Huang, N. P. Pitsianis, and X. Sun, Revision of FMM-Yukawa: An adaptive fast multipole method for screened Coulomb interactions, Comput. Phys. Commun, 181, 2206-2207, 2010.
[42] L. Ying, G. Biros, and D. Zorin, A kernel-independent adaptive fast multipole algorithm in two and three dimensions, J. Comput. Phys., 196, 591-626, 2004.
[43] J. Huang, J. Jia, and B. Zhang, FMM-Yukawa: An adaptive fast multipole method for screened coulomb interactions, Comput. Phys. Commun, 180, 2331, 2009.
[44] M. A. Kastenholz and P. H. Hunenberger, Computation of methodology-independent ionic solvation free energies from molecular simulations. II. The hydration free energy of the sodium cation, J. Chem. Phys., 124, 224501-224520, 2006.
[45] M. A. Kastenholz and P. H. Hunenberger, Computation of methodology-independent ionic solvation free energies from molecular simulations. I. The electrostatic potential in molecular liquids, J. Chem. Phys., 124, 124106-124127, 2006.
[46] B. Ni and A. Baumketner, Effect of atom- and group-based truncations on biomolecules simulated with reaction-field electrostatics, J. Mol. Model., 17, 2883-2893, 2011.
[47] J. M. Rodgersab and J. D. Weeks, Interplay of local hydrogen-bonding and long-ranged dipolar forces in simulations of confined water, PNAS, 105, 19136-19141, 2008.
[48] Z. Xu, S. Deng, and W. Cai, Image charge approximations of reaction fields in solvents with arbitrary ionic strength, J. Comput. Phys., 228, 2092-2099, 2009.
[49] D. S. Ceruttia, N. A. Baker, and J. A. McCammon, Solvent reaction field potential inside an uncharged globular protein: A bridge between implicit and explicit solvent models?, J. Chem. Phys., 127, 155101-155112, 2007.